Chemie der Erde 77 (2017) 69–79

Contents lists available at ScienceDirect

Chemie der Erde

journal homepage: www.elsevier.de/chemer

An improved EPMA analytical protocol for U-Th-Pb_{total} dating in xenotime: Age constraints from polygenetic Mangalwar Complex, Northwestern India

Pranjit Hazarika[a,b], Biswajit Mishra[a,*], Manoj Kumar Ozha[a], Kamal Lochan Pruseth[a]

[a] Department of Geology and Geophysics, Indian Institute of Technology, Kharagpur, 721302, India
[b] Department of Geological Sciences, Gauhati University, Assam-781014, India

ARTICLE INFO

Article history:
Received 20 September 2016
Received in revised form 2 January 2017
Accepted 18 January 2017
Editorial handling - Dr. T. Tomas Magna

Keywords:
Xenotime
Monazite
Electron microprobe
U-Th-Pb_{total} dating
Polygenetic ages

ABSTRACT

EPMA U-Th-Pb_{total} dating in U- and Th bearing minerals (e.g., monazite, zircon, and xenotime) is a low-cost and reliable technique used for retrieving age information from detrital, diagenetic and low to high-T metamorphic, as well as magmatic rocks. Although, the accuracy on measured ages obtained using EPMA is considered to be poor compared to isotopic ages, the superior spatial resolution, ability to integrate textural and age information by in-situ measurement, lack of sample damage and easier and cheaper data generation in EPMA make chemical dating a very valuable tool to decipher diverse petrological processes.

This contribution presents an improved analytical protocol to obtain precise estimates of U, Th and Pb concentrations in xenotime. Results were tested on monazite standard (Moacyr pegmatite, Brazil; TIMS age: 487 ± 1 Ma) as the reference material. The proposed analytical protocol has been successfully applied to achieve an analytical uncertainty of less than 10% in U, Th and Pb measurements in xenotime. The protocol was further used to resolve polygenetic xenotime ages (ca. 1.82, 1.28 and 0.93 Ga) in metapelite samples from the Mangalwar Complex, Northwestern India. Monazites in the same samples were also analyzed and found to preserve the two younger ages (i.e., ca. 1.28 and 1.0 Ga). The obtained ages from the xenotime and monazite very well corroborate with the earlier published ages from the area validating the proposed analytical protocol.

1. Introduction

Xenotime [Y(HREE)PO_4] is a common accessory mineral that hosts significant concentration of heavy rare earth elements (HREEs) and can grow in a wide range of P-T conditions (Palache et al., 1951; Giere, 1996; Spear and Pyle, 2002; Rasmussen, 2005; Rasmussen et al., 2005; Hetherington et al., 2008; Suzuki and Kato, 2008). The mineral hosts >100 parts per million (ppm) of uranium (Rasmussen et al., 2011) and excludes Pb during its growth, and once formed, it is extremely resistant to diffusional Pb loss over geological time scales at temperatures <750 °C (Dahl, 1997; Cherniak, 2006). These features make xenotime an ideal mineral for U–Th–Pb geochronology (Fletcher et al., 2000, 2004; Harrison et al., 2002; Hetherington et al., 2008; Suzuki and Kato, 2008). The ability of the mineral to record processes in wide metamorphic conditions ranging from lower greenschist to upper amphibolite facies (Hetherington et al., 2008; Rasmussen et al., 2011) and igneous events (Förster, 1998) endorses it as a robust geochronometer. Additionally, recent studies reveal that xenotime can grow in diagenetic environment (Rasmussen, 1996; Rasmussen et al., 1998) having potential to be used as a chronometer for diagenetic and low temperature hydrothermal events.

Understanding the evolution of high grade polymetamorphic terrains requires detailed petrological, geochemical and geochronological studies. Delineating geochronological evolution of polymetamorphic terrains is not straight forward, and complexities may arise as a consequence of overprinting by latest event, erasing earlier tectono-metamorphic records (e.g., Holdsworth et al., 2001; Dutch et al., 2005). Nevertheless, a promising approach to this problem is to integrate age information from growth zones of geochronometers (viz., zircon, monazite, and xenotime), which can be best approached by in-situ dating methods. In particular, monazite has received greater appreciation for preserving multiple events because of its significant response to changing metamorphic condition, while the same is not true for zircon, due to its meager response to weaker tectono-thermal events (e.g., Schenk et al.,

* Corresponding author.
E-mail address: bmgg@iitkgp.ac.in (B. Mishra).

http://dx.doi.org/10.1016/j.chemer.2017.01.010
0009-2819/

2005; Boniface et al., 2012). In spite of being competent, or indeed an alternative to monazite and/or zircon in geochronological studies, xenotime is not extensively used for dating (e.g., Suzuki and Adachi 1991; Griffin et al., 2000; Asami et al., 2002; Grew et al., 2001; Hetherington et al., 2008; Suzuki and Kato, 2008).

High spatial resolution achievable by in-situ U-Th-Pb_{total} dating using electron probe micro analyzer (EPMA) (Suzuki and Adachi, 1991) aids in obtaining texturally constrained precise age information from individual micro-domain in zoned grains (Hetherington et al., 2008). The observed concordancy in Th-Pb and U-Pb systems in monazite and xenotime (e.g., Köppel and Grünenfelder, 1971; Grauert et al., 1974; Köppel, 1974; Hawkins and Bowring, 1997) stimulate the potential of these minerals for U-Th-Pb_{total} dating. Unlike isotope methods, the accuracy and precision in the chemical ages are contentious (Cocherie et al., 2005; González-Álvarez et al., 2006; Spear et al., 2009; Jercinovic et al., 2012). However, with the understanding of appropriate limitations and taking proper precautionary measures, EPMA chemical dating can be successfully used in decoding complex tectonic events (Finger et al., 1998; Montel et al., 2000). The recent developments in chemical dating such as: (i) introduction of spectrometer incorporating larger crystals (e.g., VLPET crystal of Cameca SX-Geochron/Ultrachron, Williams et al., 2006, 2007; Hetherington et al., 2008), (ii) upgraded softwares for simultaneous analysis of U, Pb and Th in multiple spectrometers (Jercinovic and Williams, 2005; Williams et al., 2006, 2007; Spear et al., 2009), and (iii) "sub-counting" method to obtain a more precise and accurate analysis of U, Th and Pb (Spear et al., 2009; Prabhakar, 2013) are critical in order to achieve better analytical accuracy and precision. Several workers have tested and proposed improved techniques for measuring trace element concentrations in monazite (e.g., Suzuki and Adachi, 1991; Jercinovic and Williams, 2005; Williams et al., 2006, 2007; Spear et al., 2009; Jercinovic et al., 2012; Prabhakar, 2013), and have enhanced the accuracy and precision on age determinations. Because of ubiquitous occurrence of monazite in most pelitic/quartzofelspathic rocks, monazite chemical dating has received greater attention, whereas xenotime, being relatively sparse in occurrence, has not gained much consideration. Further, chemical ages obtained from xenotime have always been associated with larger errors (Chatterjee et al., 2007; Das et al., 2015) because of lower concentrations of U, Th and Pb and consequential low analytical precision. In a recent study, Hetherington et al. (2008) developed a novel analytical protocol for xenotime chemical dating and achieved very low uncertainties ($\leq$3%) on measured ages. The use of very large pentaerythritol (VLPET) crystal installed in the Cameca SX-Ultrachron at University of Massachusetts allowed the authors to achieve very high analytical precision for U, Th and Pb in the xenotime. However, it is unrealistic to acquire such high analytical precision using common electron probe micro-analyzers (Cameca SX-100, Cameca SX-Five and Jeol JXA-8230 SuperProbe) because of the absence of very large crystals, which enhance counting statistics.

In light of the advancements in analytical techniques and requirement of a protocol to date xenotime in easily accessible EPMAs (without very large crystals), in this contribution we intend to improve the analytical precision of U, Th and Pb measurements. For the same, we aim to incorporate the improved methodologies suggested by Spear et al. (2009), some of which were successfully adopted by Prabhakar (2013) for improving the analytical precision in monazite. Further, in this contribution, we present ages recorded by coexisting monazite and xenotime in same sets of samples and document the disparities in preserved age information. The comparable crystal-chemical properties of xenotime and monazite, along with negligible initial Pb content suggest that EPMA methodologies applied to monazite dating are also applicable to xenotime (Hetherington et al., 2008). Therefore, in the absence of an established xenotime standard, the protocol was tested in monazite from Moacyr pegmatite (Brazil). The small difference in matrix between LREE dominated monazite and HREE dominated xenotime should not affect U, Th and Pb measurement. This was tested by comparing results obtained for Moacyr monazite using our new protocol (for xenotime analysis) and the improved protocol of Prabhakar (2013) for monazite analysis. The calculated ages obtained using our new xenotime protocol and existing monazite protocol (Prabhakar, 2013) show significant consistency. The weighted mean ages obtained for Moacyr monazite (TIMS age = 487 ± 1 Ma; Crowley et al., 2005) using new xenotime protocol and Prabhakar's (2013) monazite protocol are 478 ± 8 Ma (n = 14) and 485 ± 8 Ma (n = 21), respectively (Fig. 1; data in Supplementary Appendix A1). The improved analytical protocol was used to resolve three age populations in xenotime at ~1.82 Ga, ~1.28 Ga, and ~0.93 Ga for the metapelites of polymetamorphic Mangalwar Complex (MC) within central Aravalli-Delhi Fold Belt (ADFB), NW India. Monazites in the same samples yielded two distinct ages at ~1.28 Ga and ~1.00 Ga. The preservation of three events in xenotime compared to two in monazite in the same samples suggests the requirement of multi-mineral chemical dating for comprehensive geochronological studies. The obtained ages and their implications are discussed in detail in later sections.

2. Analytical techniques and conditions

Three samples of metapelite from the Mangalwar Complex rocks of the ADFB were selected for the present study. Well-polished thin sections were observed under a JEOL JSM-6490 scanning electron microscope (SEM) to understand textural settings of xenotime and monazite in the samples. Major and trace element analyses of xeno-

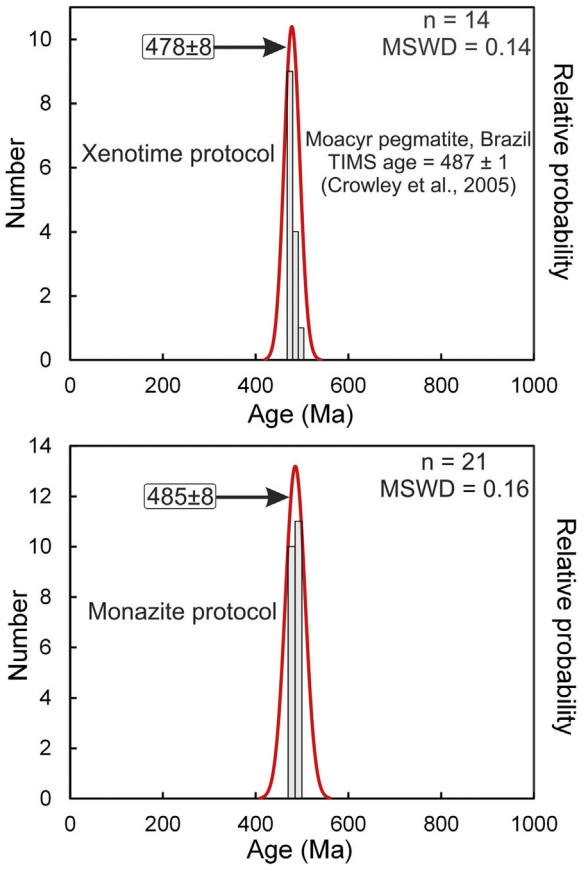

Fig. 1. Relative probability and histogram plots showing statistically significant age peak for monazite standard (Moacyr pegmatite, Brazil) using xenotime (a) and monazite protocol (b).

time and monazite were carried out using a Cameca SX-100 EPMA equipped with four wavelength dispersive spectrometers (WDS), at the Department of Geology and Geophysics, IIT Kharagpur, India. Four different crystals were used: thallium acid phthalate (TAP in WDS 1), lithium fluoride (LIF in WDS 2), pentaerythritol (PET in WDS 4) and large pentaerythritol (LPET in WDS 3). The WDS 1, 2 and 4 are fitted with low-pressure detectors, while WDS 3 is fitted with high pressure detector (P-10 gas was used for all the detectors). Both poly-propylene (in WDS 1 and 2) and Mylar (in WDS 3 and 4) windows were used as separation windows between the sample chamber and spectrometers. The CAMECA SX-100 software package was used to perform the calibration, overlap correction, quantification and age calculations.

As the accuracy of trace element measurement is a function of accurate background measurement (Spear et al., 2009), appropriate wavelength positions and PHA (pulse height analyzers) settings are critical factors for accurate age estimation. Precise measurement of trace elements in xenotime is difficult to achieve because of its compositional complexity. Peak overlap in the X-ray emission spectra of heavy REE, if not considered and corrected, may lead to substantial analytical error. The background measurement positions for all the REEs, P, Ca and Y were adopted from Hetherington et al. (2008), for Th and U were adopted from Prabhakar (2013) and for Pb were set at −1000 and +1350 after careful observation of the X-ray spectra of all the analyzed xenotime grains. In order to identify spectral interference due to existence of unexpected elements or elemental concentrations that may differ from idealized stoichiometry, X-ray spectra were obtained and monitored for all the xenotime grains prior to analyses. The PHAs were set at 'differential auto' mode for optimal results. In 'differential-auto' mode the peak-sight software sets baseline and window width automatically depending upon the energy of the measured X-ray line, and also automatically adjusts for background counts (Spear et al., 2009). All the details of analytical time, background positions, standards used and PHA settings are provided in Table 1. High precision trace element dataset for Pb, Th and U is required for extracting statistically well constrained single age from compositionally homogeneous domains. To achieve high counting precisions in EPMA, especially for very low concentrations in any sample, increasing counting time and beam current are two prerequisites. However, using high beam current and longer counting time can introduce inaccuracy due to sample damage and instrument drift. To minimize the effect of sample damage due to longer counting time, which affects background estimation, 'sub-counting' method is used in the present analytical protocol. 'Sub-counting' allows measuring peak and background in cycles by dividing the total counting time into a number of cycles. This ensures similar effect on the peak and background in the event of any surface damage (Spear et al., 2009). In addition, multi-collection enhances statistical robustness of trace element data. Thus, in the present protocol, Pb, Th and U were measured simultaneously in two spectrometers equipped with one LPET and one PET crystal. The analytical set-up in "Quanti-set" file in the Cameca PeakSight software was set in "Peak Background-Peak Background" mode for 10 cycles of counting. For example, Pb was measured in 10 cycles of 30 s at peak, and 15 s at plus-background, 15 s at minus-background in LPET, while Pb in PET was measured in 10 cycles of 20 s at peak and 10 s at plus-background and 10 s at minus-background. However, readers should note that it is unrealistic to achieve an analytical precision of more than 2% for monazites with Pb content of even 1500–2000 ppm irrespective of counting time or number of analysis being pooled (Spear et al., 2009). This roots from non-systematic variations between multiple or individual spectrometers in addition to the effect of instrumental drift. For a more detailed discussion on the errors and possible causes, the readers are referred to Spear et al. (2009). All the spot analyses were conducted at acceleration voltage of 20 kV, beam current of 150–200 nA and beam size of 1 μm using a LaB_6 electron source. Both natural and synthetic standards were used for calibration. The specific standards used for calibration are: vanadinite for Pb; UO_2 for U; ThO_2 for Th; synthetic glass containing REEs for all the REEs; apatite for P; yttrium aluminium garnet (YAG) for Y; hematite for Fe; corundum for Al and Th-glass for Si. For Pb analysis Mβ line was chosen over Mα line to avoid large overlap correction of Pb-Mα for Y-Lγ_2 and Y-Lγ_3 lines. In order to obtain better statistical precision on the Pb analyses, exponential background fit was adopted to the curvature of the background values on Pb-Mβ line (Jercinovic and Williams 2005; Williams et al., 2006, 2007). The poor count rate on Pb-Mβ line results in lower statistical precision on Pb measurement, and, because of the shorter extrapolation from background measurement position, use of similar background positions for Pb-Mβ and Pb-Mα lines results in small difference between linear and exponential fit methods of background estimation (Spear et al., 2009). Hetherington et al. (2008) have evaluated the variation in background intensity on Pb-Mβ line and Pb measurement as a function of wavelength position and background regression method on natural xenotime (#GSC6413). The results (Table 2, Hetherington et al., 2008) indicate that −1000 and +1000 are the optimal low and high background positions (in linear mode) for accurate Pb measurement resulting in date that is consistent with ID-TIMS age (983 ± 6 Ma EPMA age, Hetherington et al., 2008; 993.8 ± 0.7 Ma and 996.7 ± 0.8 Ma ID-TIMS age, Stern and Rayner, 2003; $997 \pm 0.2/0.3/1.3$ Ma and $999.7 \pm 0.3/5.0$ Ma ID-TIMS age, Schoene et al., 2006). Further, the authors observed a steady decline in measured Pb concentrations with increasing/decreasing the high/low background measurement wavelengths. Because of the sensitivity to small changes in background position, we have selected +1350 (instead of +1000), which was observed to be free from any interference. Note that such sensitivity may arise from local short-wavelength curvature of the background due to the possibility of incorporation in xenotime of unexpected elements, backscattering from which may contribute to the background intensity, as has been discussed by Hetherington et al. (2008). Counting time for Pb was 300 s at peak and 150 s at background on both sides in LPET, and 200 s at peak and 100 s at background on both sides in PET. U-Mβ line was used to measure U to avoid interference of U-Mα with Th-Mβ (Suzuki and Kato, 2008). Counting time for U-Mβ and Th-Mβ line was set at 200 s at peak and 100 s at background on both the sides in the PET crystal, while the counting time was set at 150 s at peak and 75 s at background in LPET crystal. The major spectral interferences of U-Mζ_2 and Pr-Ln line on Pb-Mβ, and Th-M_3N_4, Th-Mγ and Sm-Lβ line on U-Mβ were corrected offline during quantification. In addition to these, corrections minor spectral interferences among REEs include Yb-M_1M_2 line on P-Kα; Nd-Ll on La-Lα; Sm-Lγ on Ho-Lβ; Eu-Lβ on Er-Lα; Y-Ln on Si-Kα; Yb-M_3O_1 on Y-Lα; Th-Ll on Pr-Lβ and Th-Lα on Dy-Lα. The spot analyses were carried out away from fractures to avoid measurement of remobilized Th, U and Pb, as observed in some xenotime grains (e.g., Fig. 5a and b). K-fluorescence from K-rich phases occurring adjacent to xenotime/monazite (biotite in our sample) may lead to erroneous U estimation (Jercinovic and Williams, 2005). Thus, xenotime and monazite grains in contact with biotite were analyzed at least 10 μm inward from the margin.

3. Polygenetic xenotime and monazite from the Mangalwar Complex, Northwestern India

3.1. Geology and geochronological status of the study area

The ADFB in its central part comprises the Banded Gneissic Complex (BGC; Gupta, 1934; Heron, 1953; Fig. 2a). Based on geochronological studies, the BGC is divided into two different

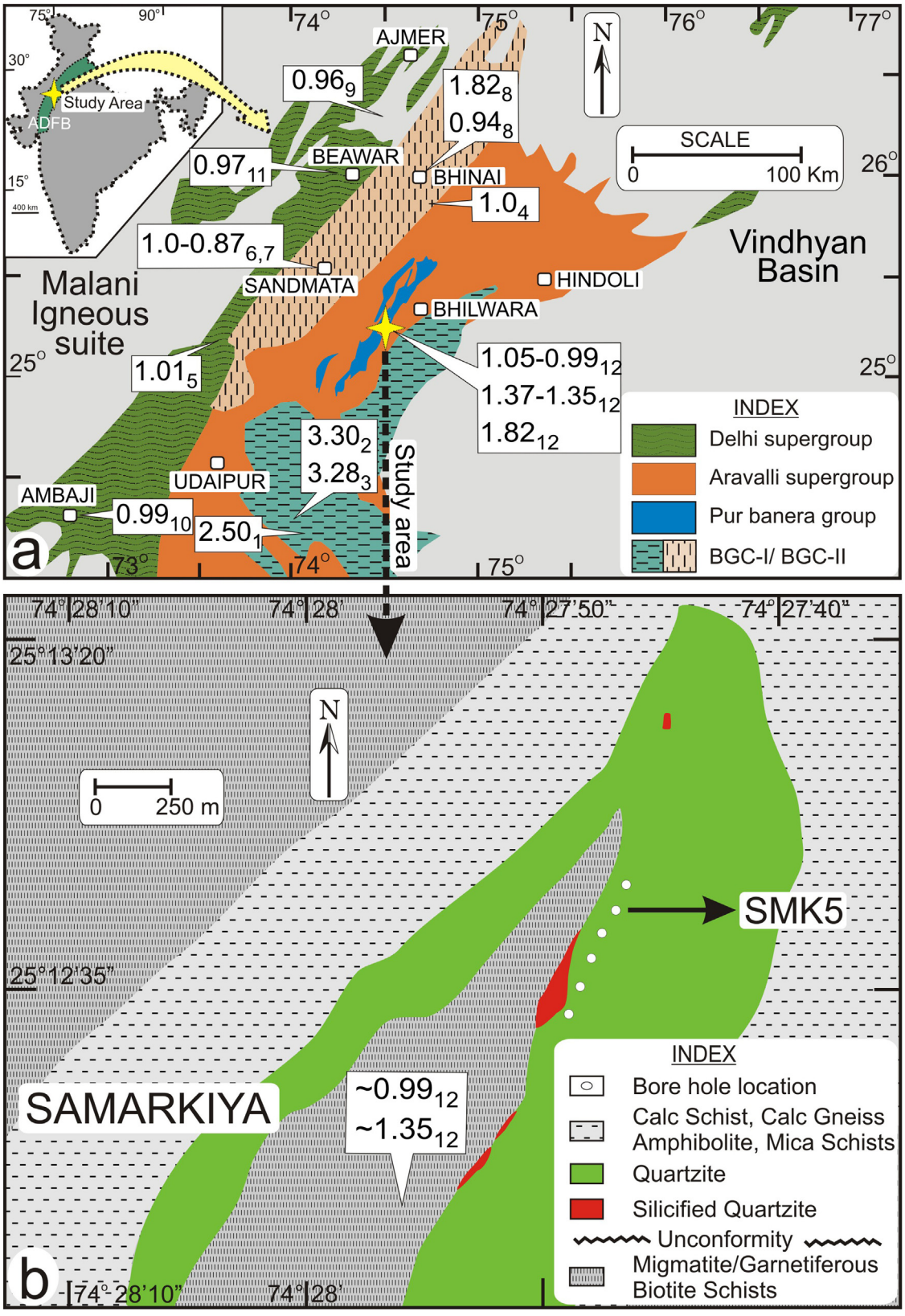

Fig. 2. Regional geological map of the Aravalli Delhi Fold Belt (ADFB), showing the distribution of different lithological components (modified after Heron 1953; Gupta et al., 1997) (a), detailed geological map of the Samarkiya area (modified after the base map of Atomic Minerals Directorate for Exploration and Research, AMDER), showing the location of the bore holes (b). The ages (in Ga) are lithology specific rather than their locations. (1) (Wiedenbeck et al., 1996a) Zircon U-Pb age; (2) (Gopalan et al., 1990) whole rock Sm-Nd age; (3) (Wiedenbeck and Goswami 1994) zircon U-Pb age; (4) (Hazarika et al., 2013) monazite U-Th-Pb$_{total}$ age; (5) (Volpe and Macdaugall 1990) whole rock Sm-Nd age; (6) (Bhowmik et al., 2010) monazite U-Th-Pb$_{total}$ age; (7) (Sarkar et al., 1989) zircon U-Pb age; (8) (Buick et al., 2006, 2010) monazite U-Th-Pb$_{total}$ and zircon U-Pb age; (9) (Tobisch et al., 1994) whole rock Rb-Sr age; (10) (Deb et al., 2001) zircon U-Pb age; (11) (Pandit et al., 2003) zircon U-Pb age; (12) (Ozha et al., 2016a) monazite U-Th-Pb$_{total}$ age.

Table 1
Major and trace element set-up for xenotime including crystal, analyzed line, background position, and calibration standard used during analysis.

Element line	Crystal	Peak time (s)	Bkg time (s)	Low Bkg	High Bkg	Slope	Calibration standard	Bkg mode	PHA mode
$Pb_{M\beta}$	LPET	300	300	−1000	1350	–	Vanadinite	Exponential	Differential Auto
$Pb_{M\beta}$	PET	200	200	−1000	1350	–	Vanadinite	Exponential	Differential Auto
$U_{M\beta}$	LPET	150	150	−996	774	–	UO_2	Linear	Differential Auto
$U_{M\beta}$	PET	200	200	−996	774	–	UO_2	Linear	Differential Auto
$Th_{M\alpha}$	LPET	150	150	–	600	1.1	ThO_2	Linear	Differential Auto
$Th_{M\alpha}$	PET	200	200	–	600	1.1	ThO_2	Linear	Differential Auto
$P_{K\alpha}$	PET	10	10	−1313	1505	–	Apatite	Linear	Integral
$Y_{L\alpha}$	TAP	20	20	–	700	1.1	YAG	Linear	Integral
$Ca_{K\alpha}$	PET	10	10	−500	500	–	Apatite	Linear	Integral
$La_{L\alpha}$	LIF	10	10	–	500	1.1	REE3	Linear	Integral
$Ce_{L\alpha}$	LIF	10	10	–	500	1.1	REE2	Linear	Integral
$Pr_{L\beta}$	PET	10	10	–	6230	1.1	REE1	Linear	Integral
$Nd_{L\beta}$	PET	10	10	–	1700	1.1	REE4	Linear	Integral
$Sm_{L\beta}$	LIF	30	30	−1187	806	–	REE3	Linear	Integral
$Eu_{L\alpha}$	LIF	30	30	−888	799	–	REE2	Linear	Integral
$Gd_{L\beta}$	LIF	30	30	−1322	1552	–	REE3	Linear	Integral
$Tb_{L\alpha}$	LIF	30	30	−627	813	–	REE4	Linear	Integral
$Dy_{L\alpha}$	LIF	20	20	−896	672	–	REE1	Linear	Integral
$Ho_{L\beta}$	LIF	30	30	−1016	1157	–	REE2	Linear	Integral
$Er_{L\alpha}$	LIF	20	20	−649	956	–	REE1	Linear	Integral
$Tm_{L\alpha}$	LIF	30	30	−754	813	–	REE2	Linear	Integral
$Yb_{L\alpha}$	LIF	20	20	−1642	590	–	REE3	Linear	Integral

* TAP: Thallium Acid Phthalate; LIF: Lithium Flouride; LLIF: Large Lithium Fluoride; PET: PentaEryThritol; LPET is Large PentaEryThritol.
Low Bkg: low-background; High Bkg: high-background.
YAG: Yttrium Aluminium Garnet.

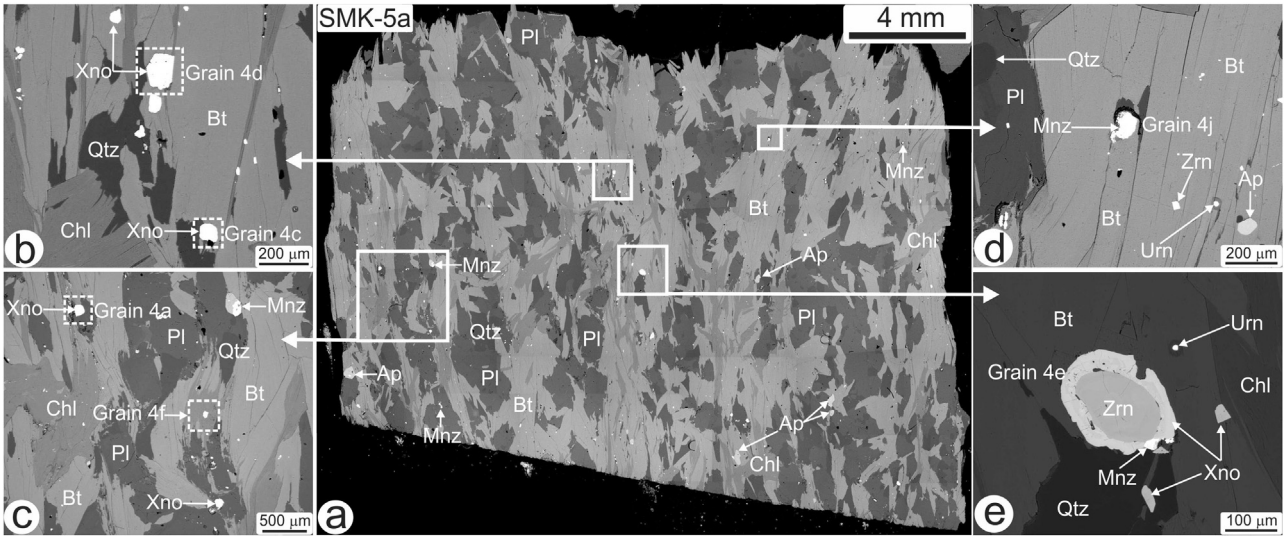

Fig. 3. Back-scattered electron (BSE) images documenting the textural occurrence of various accessory minerals (i.e., xenotime, monazite, and zircon) in sample SMK-5a.

domains, namely BGC-I and BGC-II (Fig. 2a); wherein the earlier exclusively preserves Archean ages (Wiedenbeck and Goswami, 1994; Roy and Kröner, 1996; Wiedenbeck et al., 1996a,b) and the latter is dominated by Paleo- to Neoproterozoic ages (Buick et al., 2006, 2010; Bhowmik et al., 2010) with vestiges of Archean components (Dharma Rao et al., 2011; Roy et al., 2012). The central parts of the BGC-II comprise polychronous *meta*-granitoids, amphibolites, and garnetiferous metapelites, namely the Mangalwar Complex (MC; Fig. 2a) (Heron, 1953; Gupta et al., 1997), overlain by the supracrustal metasediments of the Pur-Banera (PB) Group (Sinha-Roy et al., 1998).

Samples for present study were collected from Samarkiya area (Fig. 2b), where the metasedimentary rocks of the basement MC shares contact with the underlying supracrustal rocks of the PB (Fig. 2a). Samples collected from a bore hole (*SMK-5a, b* and *c*, 127 m depth; 25°12′38.2″N, 74°27′16.8″E; Fig. 2b) located on the eastern limb of the Samarkiya antiform (Fig. 2b) belonging to the MC (Potla Formation) were found to contain both xenotime and monazite and thus were best suited for the present study. The metasedimentary rocks of the MC witnessed three (M_1, M_2 and M_3) metamorphic events at amphibolite facies conditions (Ozha et al., 2016a). Texturally constrained monazites yielded, an age of ~1.82 Ga (U-Th-Pb_{total} method) for the high grade tectonometamorphic (M_1) event in the MC rocks (Ozha et al., 2016a) and represents the first metamorphic event in BGC-I Buick et al. (2006) obtained similar zircon U-Pb ages (~1.72 Ga) within the MC metapelites. The deformed metapelites of the MC and the PB yielded an age cluster at ~1.37 to ~1.35 Ga, corresponding to the second metamorphic event (M_2), which indicates reworking of MC rocks and first cycle of metamorphism of the PB rocks (Ozha et al., 2016a). The youngest age record of ~1.00–0.94 Ga preserved in the MC and PB rocks has been suggested to represent the last isotopic disturbance caused by amphibolite facies metamorphic overprinting (M_3) (Buick et al., 2006, 2010; Bhowmik et al., 2010; Ozha et al., 2016a).

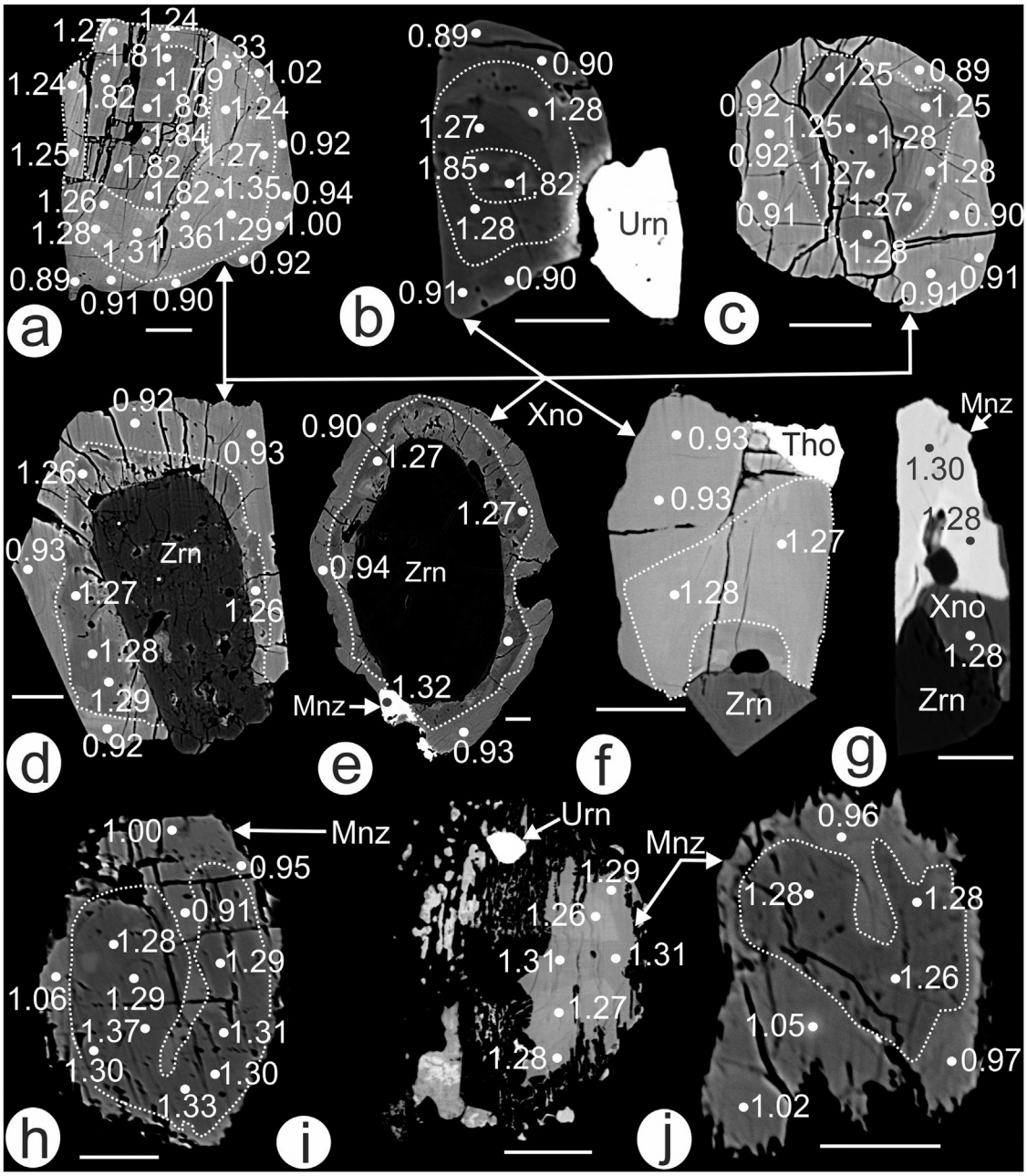

Fig. 4. Figure showing compositional zoning in BSE images of xenotime (a–g) and monazite grains (h–j) with their spot ages (in Ga). Note the coexistence of xenotime and monazite with zircon in 'g'.

3.2. Sample description and compositional zoning in xenotime and monazite

The samples *SMK-5a, b and c* are metapelites collected from a single borehole and constitute quartz, biotite, chlorite, plagioclase, rare K-feldspar and muscovite. Biotite and chlorite define the pervasive foliation (Fig. 3a). Accessory phases include apatite, xenotime, zircon, uraninite, and monazite as shown in insets in Fig. 3b–e. Xenotime and monazite are occasionally seen to occur as overgrowths over zircon (Fig. 3e).

Extensive BSE imaging in the samples reveals occurrence of numerous subhedral to anhedral grains of xenotime of varying sizes (≤150 μm in diameter, Fig. 4a–g), within and at the grain boundaries of biotite, plagioclase, chlorite and quartz (Fig. 3a). Both compositionally homogeneous and zoned grains of xenotime are found in the sample, where most of the zoned grains preserve dark grey cores surrounded by pale grey overgrowths separated by a sharp boundary (Fig. 4a–e). The irregular boundaries of the zoned/unzoned xenotime grains indicate the effect of partial resorption (cf., Aleinikoff et al., 2012) prior to recrystallization. Besides, few of the larger grains exhibit oscillatory zones (Fig. 4a and c) indicating multiple growth episodes (e.g., Viskupic and Hodges, 2001). Zircon grains were syntaxialy overgrown by xenotime displaying dark oscillatory cores and pale gray unzoned rims (Fig. 4d and e). Monazites in the studied samples are mostly homogeneous, however, occasional zoned grains are not uncommon. The patchy dark zones (≤70 μm in diameter) within the grains share sharp margins with the lighter rims in BSE images (Fig. 4h–j). Some monazite grains preserve dissolution textures as indicated by their serrated boundary (Fig. 4i and j), suggesting fluid induced alteration of the grains (Ozha et al., 2016b).

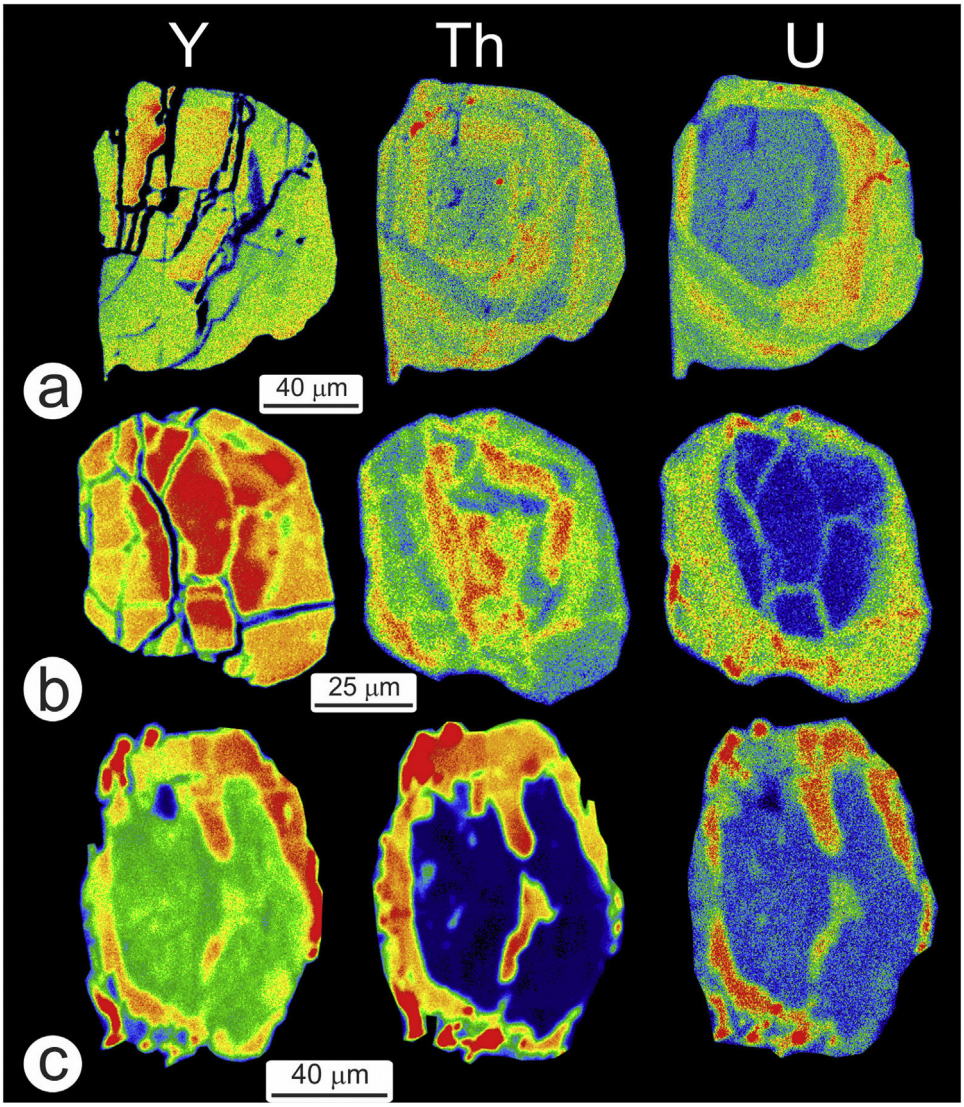

Fig. 5. Representative X-ray elemental images for Y, Th, and U showing the compositional zoning pattern in xenotime (a and b) and monazite (c).

X-ray elemental (U, Th and Y) maps illustrate distinct compositional zones within xenotime (Fig. 5a and b) and monazite grains (Fig. 5c). Grain 'a' in Fig. 5, preserves a high-Y (avg. 42.6 oxide wt.%), low-Th –U (avg. 0.40 and 0.25 oxide wt.%, respectively) relict core with irregular outline, and is mantled by an intermediate zone composed of concentric (oscillatory) sectors of variable Th-U (avg. 0.32 and 1.30 oxide wt.%, respectively), and low-Y (avg. 42.3 oxide wt.%). These oscillatory zones are subsequently rimmed by irregular domains of comparable Th-U-Y concentrations (avg. 0.30, 1.15, and 42.7 oxide wt.%, respectively). Individual spot analyses of xenotime (in Fig. 5a) reveals high ThO_2/UO_2 values (0.29–1.00) for the core as compared to the intermediate zone (0.11–0.36) and the outermost rim (0.19–0.38). Grain 'b' (Fig. 5) preserves a U-enriched locally patchy mantle over a U-depleted, Y-, Th-enriched core. BSE images (Fig. 4a and c) and Y-maps of grains 'a' and 'b' show highly fractured zones. Although the fractures are not clearly seen in the Th and U maps of grain 'a', they are distinct in the U map of grain 'b'. In contrast, both the grains (i.e., a and b) show depletion or enrichment of Th and U along the fractures, which may have significant impact on the age calculation. Thus, all the spot analyses were performed away from the fractures as depicted in Fig. 4a and c. Monazite grains in the sample preserve a Th-, U- and Y-poor subhedral to euhedral core enveloped by a Th-, U- and Y-rich rim separated by a sharp serrated boundary (e.g., Fig. 5c).

3.3. Xenotime and monazite ages

Chemical compositions, calculated ages and 2σ errors on the ages of xenotime and monazite are provided in Supplementary Appendices A2 and A3. Ages (t) for individual spot analysis were calculated using the following equation as provided in Montel et al. (1996; equation 1), where Pb, U, Th are in ppm, and λ_{232}, λ_{238}, and λ_{235} are the radioactive decay constants of ^{232}Th, ^{238}U, and ^{235}U, respectively.

$$Pb = \frac{Th}{232}[e^{\lambda_{232}t} - 1]208 + \frac{U}{238.04}0.9928 \times [e^{\lambda_{238}t} - 1]206 + \frac{U}{238.04}0.0072 \times [e^{\lambda_{235}t} - 1]207 \quad (1)$$

The errors on the calculated ages were obtained (at 95% statistical confidence) by solving equation (1) iteratively for analytical uncertainties of Th, U and Pb. Standard deviations on the measured Th, U and Pb concentrations in the Cameca SX-100 software pack-

age are obtained using the statistical formulations of Ancey et al. (1978), and are provided in detail in recent publications (Prabhakar, 2013; Appendix in Hazarika et al., 2015). Isoplot/Ex program (Ver. 3.70, Ludwig, 2000) was used to construct cumulative probability plot and "unmix ages" based on the mixture modelling approach of Sambridge and Compston (1994). Ages and associated 2σ errors obtained from spot analysis for compositionally homogeneous domains were pooled together to obtain cumulative probability distribution curve for distinct age populations. The results obtained using this method display errors on homogeneous age groups lower than the geological reality. As the errors are estimated by solving covariance matrix and confidence ellipse (Sambridge and Compston, 1994) in the Isoplot/Ex program, underlying statistical assumptions on the measurement errors such as likelihood function may provide unlikely errors. Thus, ages obtained from spot analyses of all compositional domains were plotted in UO_2^* (UO_2 plus equivalent ThO_2, for xenotime) and ThO_2^* (ThO_2 plus equivalent UO_2, for monazite) versus PbO diagram of Suzuki and Adachi (1991). Assuming similar initial Pb contents in a single generation of xenotime/monazite, distinct Th and U contents will result in a straight line (regressed pseudo-isochron) defined by the equation $PbO = m \times UO_2^* + b$ (for xenotime) and $PbO = m \times ThO_2^* + b$ (for monazite), where b represents the initial Pb content. Thus, a significant initial Pb content in studied xenotime/monazite would result in deviation of the intercept of regressed line from origin.

A total of 115 spot analyses were carried out in a number of selected xenotime grains using the new analytical protocol. Ages from spot analyses range from 880 to 1897 Ma with corresponding 2σ errors between 39 and 189 Ma (Supplementary Appendix A2). Relative probability plot shows three age peaks at ~1850 Ma (14% of the total), ~1270 Ma (31% of the total) and ~930 Ma (51% of the total) (Fig. 6a). The oldest age at ~1.85 Ga represents weighted average of 20 spot analyses obtained exclusively from the cores of zoned grains (Fig. 4a and b). The intermediate age of ~1.27 Ga (Fig. 6a) constitute 36 spot analyses, and are confined to the intermediate zone (Fig. 3a), occasionally as core of zoned grains where the oldest age is missing (Fig. 3c), and as overgrowth zones at the contact of zircon (Fig. 4d and e). The youngest age population of ~0.93 Ga is obtained from 59 spot analyses and is restricted to the rims of the zoned grains (Fig. 4a–e) and occasionally within discrete homogeneous grains. In general, the youngest age population in xenotime has been obtained from the rims of zoned grains, as seen from the BSE (Fig. 4a–f) and X-ray element images (Fig. 5a and b). The CHIME ages as calculated using the computer program of Kato et al. (1999 http://www.nendai.nagoya-u.ac.jp/gsd/CHIME/) are 1790 ± 107, 1279 ± 23 and 921 ± 43 Ma (Fig. 6b). The regressed lines (pseudo-isochron) for distinct age populations have very low ordinate intercept values (<0.005) in the UO_2^*-PbO plot, indicating negligible initial Pb content in studied xenotime grains. A total of 50 spot ages (Supplementary Appendix A3) were acquired from selected monazite grains using the improved protocol as provided in Prabhakar (2013). The relative probability plot shows three distinct age peaks at ~1280 Ma (68% of the total) ~1060 Ma (14% of the total) and ~950 Ma (18% of the total) (Fig. 6c). The calculated CHIME ages with respective 2σ errors are 1261 ± 24, 1046 ± 47 and 945 ± 21 Ma (Fig. 6d). The very low PbO-intercept values (−0.08) for the two regressed lines (pseudo-isochrons) in the ThO_2^*-PbO plot (Fig. 6d) substantiate the absence of initial lead in the studied monazite grains (Kato et al., 1999). The cores of the zoned grains along with the compositionally homogeneous monazites preserve the older age (~1.28 Ga), while the bulk of the latter two age clusters (~1.05 Ga and ~0.95 Ga) comes from the rims of the zoned grains (Fig. 4h and j). Although not ubiquitous, two distinct low-Th, −U and high-Th, −U zones within monazite rim (Fig. 5c) correspond-

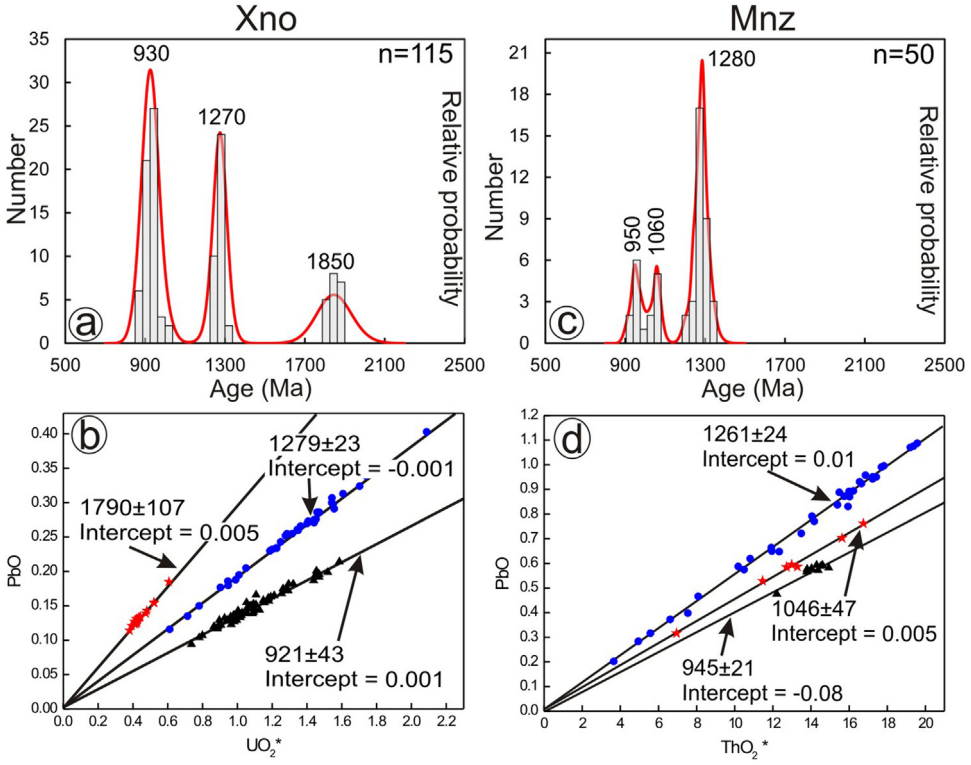

Fig. 6. Relative probability and histogram plots showing three statistically significant age peaks (in Ma) in xenotime and monazite (a and c, respectively). CHIME ages for xenotime and monazite are shown in UO2* (for xenotime)/ThO2* (for monazite) versus PbO plots (b and d, respectively). Note the very low intercept values (< 0.01) of the regressed isochrons, indicating negligible initial Pb contents.

ingly preserves spot ages representing the age cluster ~1.05 Ga and ~0.95 Ga (6d; Supplementary Appendix A3).

3.4. Age implications

Xenotime in the samples preserve three Proterozoic age records at ca. 1.80, 1.27, and 0.93. Although, monazite in the same samples preserve three ages (~1.28 and ~1.05, and 0.95 Ga), the oldest Paleoproterozoic age record (~1.80 Ga) is distinctly absent in them. The oldest Late Palaeoproterozoic age (~1.80 Ga) is invariably preserved within relict cores of xenotime grains, while the younger two ages (~1.27 and ~0.93 Ga) are recorded in the overgrowth (Fig. 4a and b) zones. Ozha et al. (2016a) reported xenotime grains confined to the relict garnet cores together with metamorphic monazites (ca. 1.82 Ga, U-Th-Pb_{total} age) within the MC metapelites (sample MC9, Fig. 2b in Ozha et al., 2016a). The ca. 1.82 Ga age has been suggested to represent the first metamorphic event (M_1, with a peak P-T of ~5.5 kbar and 520–550 °C) in the M Buick et al. (2010) have also reported similar ages (~1.82 Ga) for metamorphic monazites from the MC metapelites in the Bhinai area (see, Fig. 2a). Thus, in the light of the published ages from the MC, we assign our oldest age (ca. 1.80 Ga) to represent xenotime growth in the M_1 metamorphic event.

The Mesoproterozoic age (~1.28–1.27 Ga, Fig. 6) is invariably found preserved within xenotime and in the cores of the monazite grains. Monazite preserving the intermediate age (i.e., ~1.28 Ga) locally shows dissolution textures (Figs. 3c, 4i and j), wherein coronal growth of apatite, huttonite and coffinite over monazite were also seen (see Fig. 8; Ozha et al., 2016b); thus indicating fluid-assisted monazite recrystallization. Similar coronal growths of apatite, allanite and huttonite over monazite were reported from Granatspitz massif, central eastern Alps (Finger et al., 1998) and Tso Morari complex, NW Himalayas (Upadhyay and Pruseth, 2012) in amphibolite facies assemblages within metamorphosed granitoid. Ozha et al. (2016a) established record of a ~1.35 Ga upper-amphibolite facies (peak P-T of ~7.5 kbar and 580–660 °C) tectonometamorphic event (i.e., M_2) in the Pur-Banera area. Thus, we infer that the intermediate age population (~1.28–1.27 Ga) within xenotime and monazite most likely represents a post-peak metamorphic hydrothermal event. This inference is further consistent with the chemical dates of uraninite at ~1.25 Ga (Ozha et al., under review), representing a hydrothermal event in the Samarkiya area during post-peak retrogression.

The rims of xenotime and monazite grains in the samples preserve Early Neoproterozoic ages (~1.05–0.90 Ga), with a distinct age cluster at ~0.95–0.93 Ga (Fig. 6a and c). Besides, an older (~1.05 Ga) age is obtained from monazite. The age clusters of ~1.05 and ~0.95–0.93 Ga are indistinguishable from the age of the peak metamorphism *(M_3)* as recorded from the rocks of the PB (~1.05 Ga) and the MC (~0.98 Ga) (Ozha et al., 2016a). In addition, the ~1.05 Ga age is also consistent with previously published U-Pb and U-Th-Pb_{total} ages from monazite (~0.97–0.93 Ga, Buick et al., 2010; ~0.98–0.95 Ga, Bhowmik et al., 2010; ~1.00 Ga, Hazarika et al., 2013) and zircon U-Pb ages (~1.05–0.95 Ga; Buick et al., 2006) within the MC metapelites. Although, the obtained discrete age clusters are respectively found preserved within distinct compositional zones of xenotime and monazite, it is difficult to discriminate them with respect to different tectonic events. The ages at ~1.05 and ~0.95–0.93 Ga constitute spot analyses from the rims of the xenotime and monazite grains and most likely indicate the same tectonometamorphic event (M_3 of Ozha et al., 2016a). Previous studies have linked this Neoproterozoic event to the global ca. 1.0 Ga Grenvillian orogeny, which represents the amalgamation of Rodinia supercontinent in the ADFB (Bhowmik et al., 2010; Ozha et al., 2016a). Thus, we interpret the Early Neoproterozoic age clusters (~1.05 and ~0.95–0.93 Ga) yielded by xenotime and monazite in the present study to represent episodes related to the pervasive Grenvillian overprinting in the area and further supports Rodinia amalgamation in the central Rajasthan.

4. Concluding remarks

The present study documents that precise U, Th and Pb measurement in xenotime can be attained by analyzing simultaneously in multiple spectrometers (PET and LPET crystals) in sub-counting mode and adjusting the pH A in “differential-auto” mode. Higher counting time (for U, Th, and Pb) in PET and LPET crystals and higher beam current (150–200 nA) reduce statistical uncertainties. This study substantiates the role and the efficacy of EPMA in dating small grains/zones as compared to isotopic techniques (viz. SHRIMP, LA-ICP-MS) that require larger grains. In spite of low-Th content in natural xenotime, precise ages can be obtained using our improved analytical method in readily accessible EPMA and thus xenotime chemical (U-Th-Pb_{total}) dating may be considered as a potential reconnaissance geochronological tool. Xenotime in metapelitic samples from the ADFB preserve significant geological event (ca. 1.80 Ga) which was found missing in the coexisting monazite. Thus, xenotime chemical dating offers reliable and robust age information irrespective of the occurrence of monazite. The results obtained from this study endorse the use of multiple geochronometers for obtaining comprehensive age information in terrains with complex evolutionary history.

Acknowledgements

PH and MKO respectively thank the Council of Scientific and Industrial Research, India and IIT Kharagpur for funding research fellowships. SEM-BSE imaging and EPMA data were generated by the equipment procured through a Department of Science and Technology (DST-India) funding (IR/S4/ESF-08/2005) to the Department of Geology and Geophysics, IIT Kharagpur. Saptarshi Sinha is thanked for his help in EMP analysis. The authors thank many constructive comments by two anonymous journal reviewers and editorial suggestions by Tomas Magna and Alex Deutsch.

Appendix A. Supplementary data

Supplementary data associated with this article can be found, in the online version, at http://dx.doi.org/10.1016/j.chemer.2017.01.010.

References

Aleinikoff, J.N., Hayes, T.S., Evans, K.V., Mazdab, F.K., Pillers, R.M., Fanning, C.M., 2012. SHRIMP U-Pb ages of xenotime and monazite from the Spar Lake red bed-associated Cu-Ag deposit, Western Montana: implications for ore genesis. Econ. Geol. 107, 1251–1274.

Ancey, M., Bastenaire, F., Tixer, R., 1978. Application des methodes stastistiques en microanalyse. In: Maurice, F., Meny, L., Tixer, R. (Eds.), Microanalyse, microscopie electronique a balayae. Leś Editions du Physicien. Orsay, pp. 323–347.

Asami, M., Suzuki, K., Grew, E.S., 2002. Chemical Th-U-total Pb dating by electron microprobe analysis of monazite, xenotime and zircon from the Archean Napier Complex, East Antarctica: evidence for ultra-high-temperature metamorphism at 2400 Ma. Precambrian Res. 114, 249–275.

Bhowmik, S.K., Bernhardt Heinz, J., Dasgupta, S., 2010. Grenvillian age high-pressure upper amphibolite-granulite metamorphism in the Aravalli-Delhi Mobile Belt, Northwestern India: new evidence from monazite chemical age and its implication. Precambrian Res. 78, 168–184.

Boniface, N., Schenk, V., Appel, P., 2012. Paleoproterozoic eclogites of MORB-type chemistry and three Proterozoic orogenic cycles in the Ubendian Belt (Tanzania): evidence from monazite and zircon geochronology, and geochemistry. Precambrian Res. 192, 16–33.

Buick, I.S., Allen, C., Pandit, M., Rubatto, D., Hermann, J., 2006. The proterozoic magmatic and metamorphic history of the banded gneiss complex, Central Rajasthan, India : LA-ICP-MS U-Pb zircon constraints. Precambrian Res. 151, 119–142.

Buick, I.S., Clark, C., Rubatto, D., Hermann, J., Pandit, M.K., Hand, M., 2010. Constraints on the Proterozoic evolution of the Aravalli-Delhi Orogenic belt (NW India) from monazite geochronology and mineral trace element geochemistry. Lithos 120, 511–528.
Chatterjee, N., Mazumdar, A.C., Bhattacharya, A., Saikia, R.R., 2007. Mesoproterozoic granulites of the Shillong–Meghalaya Plateau: evidence of westward continuation of the Prydz Bay Pan-African suture into Northeastern India. Precambrian Res. 152, 1–26.
Cherniak, D.J., 2006. Pb and rare earth element diffusion in xenotime. Lithos 88, 1–14.
Cocherie, A., Be Mezeme, E., Legendre, O., Fanning, C.M., Faure, M., Rossi, P., 2005. Electron-microprobe dating as a tool for determining the closure of Th-U-Pb systems in migmatitic monazites. Am. Miner. 90, 607–618.
Crowley, J.L., Chatterjee, N., Bowring, S.A., Sylvester, P.J., Myers, J.S., Searle, M.P., 2005. U–(Th)–Pb dating of monazite and xenotime by EMPA, LAICPMS, and IDTIMS: examples from the Yilgarn Craton and Himalayas. Proceedings of the 15th Annual Goldschmidt Conference, A19, Abstracts.
Dahl, P.S., 1997. A crystal-chemical basis for Pb retention and fission-track annealing systematics in U-bearing minerals, with implications for geochronology. Earth Planet. Sci. Lett. 150, 277–290.
Das, S., Shukla, S., Bhattacharjee, S., Mitra, S.K., 2015. Age constraints of udayagiri domain of Nellore Schist belt by xenotime dating around Pamuru, Prakasam district, Andhra Pradesh. J. Geol. Soc. India 85, 289–298.
Deb, M., Thorpe, R.I., Kristic, D., Corfu, F., Davis, D.W., 2001. Zircon U-Pb and galena Pb isotope evidence for an approximate 1.0 Ga terrane constituting the western margin of the Aravalli-Delhi orogenic belt, Northwestern India. Precambrian Res. 108, 195–213.
Dharma Rao, C.V., Santosh, M., Purohit, R., Wang, J., Jiang, X., Kusky, T., 2011. LA–ICP–MS U–Pb zircon age constraints on the Paleoproterozoic and Neoarchean history of the Sandmata Complex in Rajasthan within the NW Indian Plate. J. Asian Earth Sci. 42, 286–305.
Dutch, R.A., Hand, M., Clark, C., 2005. Cambrian reworking of the southern Australian Proterozoic Curnamona Province: constraints from regional shear-zone systems. J. Geol. Soc. Lond. 162, 763–775.
Förster, H.-J., 1998. The chemical composition of REE-Y-Th-U-rich accessory minerals in peraluminous granites of the Erzgebirge-Fichtelgebirge region, Germany, Part II: Xenotime. Am. Mineral. 83, 1302–1315.
Finger, F., Broska, I., Roberts, M.P., Schermaier, A., 1998. Replacement of primary monazite by apatite-allanite-epidote coronas in an amphibolite facies granite gneiss from the eastern Alps. Am. Mineral. 83, 248–258.
Fletcher, I.R., Rasmussen, B., McNaughton, N.J., 2000. SHRIMP U–Pb geochronology of authigenic xenotime and its potential for dating sedimentary basins. Aust. J. Earth Sci. 47, 845–859.
Fletcher, I.R., McNaughton, N.J., Aleinikoff, J.A., Rasmussen, B., Kamo, S.L., 2004. Improved calibration procedures and new standards for U–Pb and Th–Pb dating of Phanerozoic xenotime by ion microprobe. Chem. Geol. 209, 295–314.
Giere, R., 1996. Formation of rare earth minerals in hydrothermal systems. In: Jones, A.P., Wall, F., Williams, C.T. (Eds.), Rare Earth Minerals: Chemistry, Origin and Ore Deposits, vol. 7, pp. 105–150, Mineralogical Society Series.
González-Álvarez, I., Kusiak, M.A., Kerrich, R., 2006. A trace element and chemical Th-U total Pb dating study in the lower Belt-Purcell Supergroup, Western North America: provenance and diagenetic implications. Chem. Geol. 230, 140–160.
Gopalan, K., Macdougall, J.D., Roy, A.B., Murali, A.V., 1990. Sm–Nd evidence for 3.3 Ga old rock in Rajasthan, North-Western India. Precambrian Res. 48, 287–297.
Grauert, B., Hänny, R., Soptrajanova, G., 1974. Geochronology of polymetamorphic and anatectic gneiss region: the Moldanubicum of the area Lam-Deggendorf Eastern Bavaria, Germany. Contrib. Mineral. Petrol. 45, 37–63.
Grew, E.S., Suzuki, K., Asami, M., 2001. CHIME ages of xenotime, monazite and zircon from beryllium pegmatites in the Napier Complex, Khmara Bay, Enderby Land, East Antarctica. Polar Geosci. 14, 99–118.
Griffin, B.J., Forbes, D., McNaughton, N.J., 2000. Evaluation of dating of diagenetic xenotime by electron microprobe. Microsc. Microanal. 6, 408–409.
Gupta, S.N., Arora, Y.K., Mathur, R.K., Iqbaluddin, Prasad, B., Sahai, T.N., Sharma, S.B., 1997. The Precambrian geology of the Aravalli region, southern Rajasthan and north-eastern Gujarat. Mem. Geol. Surv. India Hyderabad 123, 262.
Gupta, B.C., 1934. The geology of central Mewar. Mem. Geol. Surv. India 65, 107–168.
Harrison, T.M., Catlos, E.J., Montel, J.M., 2002. U-Th-Pb dating of phosphate minerals. Rev. Mineral. Geochem. 48, 524–558.
Hawkins, D.P., Bowring, S.A., 1997. U-Pb systematics of monazite and xenotime: case studies from the Paleoproterozoic of the Grand Canyou, Arizona. Contrib. Mineral. Petrol. 127, 87–103.
Hazarika, P., Upadhyay, D., Mishra, B., 2013. Contrasting geochronological evolution of the Rajpura-Dariba and Rampura-Agucha metamorphosed Zn-Pb deposit, Aravalli-Delhi belt, India. J. Asian Earth Sci. 73, 329–339.
Hazarika, P., Mishra, B., Pruseth, K.L., 2015. Diverse tourmaline compositions from orogenic gold deposits in the Hutti-Maski greenstone belt, India: implications for sources of ore-forming fluids. Econ. Geol. 110, 337–353.
Heron, A.M., 1953. The geology of central Rajputana. Mem. Geol. Surv. India 79, 389.
Hetherington, C.J., Jercinovic, M.J., Williams, M.L., Mahan, K., 2008. Understanding geologic processes with xenotime: composition, chronology, and a protocol for electron probe microanalysis. Chem. Geol. 254, 133–147.
Holdsworth, R.E., Handa, M., Miller, J.A., Buick, I.S., 2001. Continental reactivation and reworking: an introduction. Geol. Soc. Lond. 184, 1–12, Special Publications.
Jercinovic, M.J., Williams, M.L., 2005. Analytical perils (and progress) in electron microprobe trace element analysis applied to geochronology: back-ground acquisition, interferences, and beam irradiation effects. Am. Mineral. 90, 526–546.
Jercinovic, M.J., Williams, M.L., Allaz, J., Donovan, J.J., 2012. Trace analysis in EPMA. IOP Conf. Ser.: Mater. Sci. Eng. 32, 12012.
Köppel, V., Grünenfelder, M., 1971. A study of inherited and newly formed zircons from paragneisses and granitised sediments of the Strona-Ceneri- Zone (Southern Alps). Schweiz. Mineral. Petrogr. Mitt. 51, 385–409.
Köppel, V., 1974. Isotopic U-Pb ages of monazites and zircons from the crust-mantle transition and adjacent units of the Iveria and Ceneri zones (Southern Alps, Italy). Contrib. Mineral. Petrol. 43, 55–70.
Kato, T., Suzuki, K., Adachi, M., 1999. Computer program for the CHIME age calculation. J. Earth Planet. Sci. 46, 49–56.
Ludwig, K.R., 2000. User's Manual for Isoplot/ex Rev. 2.49: A Geochronological Toolkit for Microsoft Excel. Berkeley Geochronology Center, pp. 1–56, Special Publication 1a.
Montel, J.M., Foret, S., Veschambre, M., Nicollet, C., Provost, A., 1996. Electron microprobe dating of monazite. Chem. Geol. 131, 37–53.
Montel, J.M., Kornprobst, J., Vielzeuf, D., 2000. Preservation of old U-Th-Pb ages in shielded monazite: example from the Beni Bousera Hercynian kinzigites (Morocco). J. Metamorph. Geol. 18, 335–342.
Ozha, M.K., Mishra, B., Hazarika, P., Jeyagopal, A.V., Yadav, G.S., 2016a. EPMA monazite geochronology of the basement and supracrustal rocks within the Pur-Banera basin, Rajasthan: evidence of Columbia breakup in Northwestern India. J. Asian Earth Sci. 117, 284–303.
Ozha, M.K., Mishra, B., Jeyagopal, A.V., 2016b. Reaction aureoles around uraninites within biotite and plagioclase: evidence of low temperature sequential fluid alteration and LREE-mobilization from monazite. Mineral. Mag. 80, 1556–17584.
Palache, C., Berman, H., Frondel, C., 1951. The System of Mineralogy, vol. II., 7th ed. Wiley, New York.
Pandit, M.K., Carter, L.M., Ashwal, L.D., Tucker, R.D., Torsvik, T.H., Jamtveit, B., Bhusan, S.K., 2003. Age petrogenesis and significance of 1 Ga granitoids and related rocks from the Sendra area, Aravalli craton, NW India. J. Asian Earth Sci. 22, 363–381.
Prabhakar, N., 2013. Resolving poly-metamorphic Paleoarchean ages by chemical dating of monazites using multi-spectrometer U, Th and Pb analyses and sub-counting methodology. Chem. Geol. 347, 255–270.
Rasmussen, B., Buick, R., Taylor, W.R., 1998. Removal of oceanic REE by authigenic precipitation of phosphatic minerals. Earth Planet. Sci. Lett. 164, 135–149.
Rasmussen, B., Sheppard, S., Fletcher, I.R., 2005. Isotopic dating of the migration of a low-grade metamorphic front during orogenesis. Geology 33, 773–776.
Rasmussen, B., Fletcher, I.R., Muhling, J.R., 2011. Response of xenotime to prograde metamorphism. Contrib. Mineral. Petrol. 162, 1259–1277.
Rasmussen, B., 1996. Early-diagenetic REE-phosphate minerals (florencite, gorceixite, crandallite, and xenotime) in marine sandstones; a major sink for oceanic phosphorus. Am. J. Sci. 296, 601–632.
Rasmussen, B., 2005. Radiometric dating of sedimentary rocks: the application of diagenetic xenotime geochronology. Earth Sci. Rev. 68, 197–243.
Roy, A.B., Kröner, A., 1996. Single zircon evaporation ages constraining the growth of the Archaean Aravalli craton, northwestern Indian shield. Geol. Mag. 133, 333–342.
Roy, A.B., Kröner, A., Rathore, S., Laul, V., Purohit, R., 2012. Tectono-metamorphic and geochronologic studies from Sandmata Complex, Northwest Indian shield: implications on exhumation of late-palaeoproterozoic granulites in an archaean-early palaeoproterozoic granite-gneiss terrane. J. Geol. Soc. India 79, 323–334.
Sambridge, M.S., Compston, W., 1994. Mixture modeling of multicomponent data sets with application to ion probe zircon ages. Earth Planet Sci. Lett. 128, 373–390.
Sarkar, G., Barman, T., Corfu, F., 1989. Timing of continental arc magmatism in northwest India: evidence from U-Pb Zircon geochronology. J. Geol. 97, 607–612.
Schenk, V., Appel, P., Jöns, N., Loose, D., Schumann, A., Wegner, H., 2005. Pan-African reworking of the northeastern corner of the Congo Craton in Uganda. In: Wingate, M.T.D., Pisarevsky, S.A. (Eds.), Supercontinents and Earth Evolution Symposium, 81. Geol Soc. Australia, p. 100.
Schoene, B., Crowley, J.L., Condon, D.J., Schmitz, M.D., Bowring, S.A., 2006. Reassessing the uranium decay constants for geochronology using ID-TIMS U–Pb data. Geochim. Cosmochim. Acta 70, 426–445.
Sinha-Roy, S., Malhotra, G., Mohanty, M., 1998. Geology of Rajasthan. Geological Society of India, Bangalore, pp. 278–$9.
Spear, F.S., Pyle, J.M., 2002. Apatite, monazite, and xenotime in metamorphic rocks. Rev. Mineral. Geochem. 48, 293–335.
Spear, F.S., Pyle, J.M., Cherniak, D., 2009. Limitations of chemical dating of monazite. Chem. Geol. 266, 218–230.
Stern, R., Rayner, N., 2003. Ages of Several Xenotime Megacrysts by ID-TIMS: Potential Reference Materials for Ion Microprobe U–Pb Geochronology. Geological Survey of Canada, Ottawa.
Suzuki, K., Adachi, M., 1991. Precambrian provenance and Silurian metamorphism of the Tsubonasawa paragneiss in the South Kitakami terrane Northwest Japan, revealed by the chemical Th-U-total Pb isochron ages of monazite, zircon and xenotime. Geochem. J. 25, 357–376.

Suzuki, K., Kato, T., 2008. CHIME dating of monazite, xenotime, zircon and polycrase: protocol, pitfalls and chemical criterion of possibly discordant age data. Gondwana Res. 14, 569–586.
Tobisch, O.T., Collerson, K.D., Bhattacharya, T., Mukhopadhyay, D., 1994. Structural relationship and Sm-Nd isotopic systematics of polymetamorphic granite gneisses and granitic rocks from central Rajasthan: implications for the evolution of Aravalli craton. Precambrian Res. 65, 319–339.
Upadhyay, D., Pruseth, K.L., 2012. Fluid-induced dissolution breakdown of monazite from Tso Morari complex, NW Himalayas: evidence for immobility of trace elements. Contrib. Mineral. Petrol. 164, 303–316.
Viskupic, K., Hodges, K.V., 2001. Monazite–xenotime thermochronometry: methodology and an example from the Nepalese Himalaya. Contrib. Mineral. Petrol. 141, 233–247.
Volpe, A.M., Macdaugall, J.D., 1990. Geochemistry and isotopic characteristics of mafic (Phulad Ophiolite) and related rocks in the Delhi Supergroup Rajasthan, India: implications for rifting in the Proterozoic. Precambrian Res. 48, 167–191.
Wiedenbeck, M., Goswami, J.N., 1994. An ion-probe single zircon Pb age from the Mewar Gneiss at Jhamarkotra, Rajasthan. Geochim. Cosmochim. Acta. 58, 2135–2141.
Wiedenbeck, M., Goswami, J.N., Roy, A.B., 1996a. Stabilisation of the Aravalli craton of the north-western India at 2.5 Ga.: an ion-microprobe zircon study. Chem. Geol. 129, 325–340.
Wiedenbeck, M., Goswami, J.N., Roy, A.B., 1996b. An ion microprobe study of single zircons from the Amet granite, Rajasthan. J. Geol. Soc. India 48, 127–137.
Williams, M.L., Jercinovic, M.J., Goncalves, P., Mahan, K., 2006. Format and philosophy for collecting, compiling, and reporting microprobe monazite ages. Chem. Geol. 225, 1–15.
Williams, M.L., Jercinovic, M.J., Hetherington, C.J., 2007. Microprobe monazite geochronology: understanding geologic processes by integrating composition and chronology. Ann. Rev. Earth Planet. Sci. 35, 137–175.